MOX-Report No. 19/2016

Computational comparison between Newtonian and non-Newtonian blood rheologies in stenotic vessels

Guerciotti, B.; Vergara, C.

MOX, Dipartimento di Matematica
Politecnico di Milano, Via Bonardi 9 - 20133 Milano (Italy)

mox-dmat@polimi.it http://mox.polimi.it

Computational comparison between Newtonian and non-Newtonian blood rheologies in stenotic vessels

Bruno Guerciotti[1] Christian Vergara[1]

[1] MOX - Department of Mathematics, Politecnico di Milano, Piazza Leonardo da Vinci 32, 20133 Milano, Italy

Abstract

This work aims at investigating the influence of non-Newtonian blood rheology on the hemodynamics of 3D patient-specific stenotic vessels, by means of a comparison of some numerical results with the Newtonian case. In particular, we consider two carotid arteries with severe stenosis and a stenotic coronary artery treated with a bypass graft, in which we virtually vary the degree of stenosis. We perform unsteady numerical simulations based on the Finite Element method using the Carreau-Yasuda model to describe the non-Newtonian blood rheology. Our results show that velocity, vorticity and wall shear stress distributions are moderately influenced by the non-Newtonian model in case of stenotic carotid arteries. On the other hand, we observed that a non-Newtonian model seems to be important in case of stenotic coronary arteries, in particular to compute the *relative residence time* which is greatly affected by the rheological model.

Keywords: stenotic vessels; non-Newtonian rheology; computational fluid-dynamics

1 Introduction

Blood is a two-phase mixture comprising various types of formed elements (red blood cells, white blood cells, platelets) suspended in an aqueous solution of organic molecules, proteins, and salts called plasma. Because of this multi-component nature, blood exhibits complex rheological properties [1, 3]. In particular, several experimental investigations showed that blood features a so-called *shear-thinning* behaviour, that is, its viscosity decreases with increasing shear rates, reaching a nearly constant value of approximately 0.035 poise only for shear rates grater than $200s^{-1}$ [7].

In computational fluid-dynamics, the assumption of Newtonian flow (i.e. constant viscosity) is generally accepted for blood flow in large-sized arteries, such as the aorta, where the shear rates are high, while the non-Newtonian behavior of blood has to be taken into account in small vessels like the capillaries [3]. For medium-sized vessels, such as the carotid arteries or the coronary arteries, the validity of the Newtonian hypothesis is still not completely clear,

Table 1: Review of the literature regarding computational studies in carotid and coronary arteries using non-Newtonian models

	Arterial vessel	Geometry	Non-Newtonian model
Box et al [4]	non-sten carotids	Ideal, 3D	Carreau-Yasuda
Boyd et al [5]	non-sten carotids	Real, 2D	Carreau-Yasuda
Gijsen et al [10]	non-sten carotids	Ideal, 3D	Carreau-Yasuda
Perktold et al [23]	non-sten carotids	Ideal, 3D	Casson
Razavi et [24]	stenotic carotids	Ideal, 2D	6 different models[a]
Shirmer et al [27]	stenotic carotids	Real, 3D	Carreau
Stroud et al [30]	stenotic carotids	Real, 2D	Power Law
Valencia et al [31]	non-sten carotids	Real, 3D	Herschel-Bukley
Chen et al [6]	stenotic coronaries	Ideal, 3D	Carreau-Yasuda
Jeong et al [13]	non-sten coronaries	Ideal, 2D	Carreau
Johnston et al [14]	non-sten coronaries	Real, 3D	Generalised Power Law
Kabinejadian et al [15]	non-sten coronaries	Ideal, 3D	Carreau-Yasuda
Liu et al [20]	non-sten coronaries	Real, 3D	Power Law
Soulis et al [29]	non-sten coronaries	Real, 3D	7 different models[b]
Vimmr et al [33]	stenotic coronaries	Real, 3D	Carreau-Yasuda

[a] Power Law, Carreau, Carreau-Yasuda, Modified-Casson, Generalized Power Law, Walburn-Schneck
[b] Carreau, Carreau-Yasuda, Power Law, Non-Newtonian Power Law, Generalized Power Law, Casson, Walburn-Schneck

especially in the stenotic case. In addition to this, presently there is no universal agreement upon the correct model to represent the viscous properties of blood [26]. For these reasons, modelling of blood's non-Newtonian behavior is increasingly being performed and different non-Newtonian models have been used in order to study their effects on blood flow characteristics (e.g. flow field, secondary flow patterns, wall shear stresses).

We report in Table 1 the main computational studies regarding the use of non-Newtonian models in (possibly stenotic) carotid and coronary arteries, either in ideal or real (i.e. patient-specific) geometries. Most of the literature deals with healthy (i.e. non-stenotic) geometries, see [4, 5, 10, 23, 31] for carotid arteries and [13, 14, 20, 29] for coronary arteries, whereas studies on stenotic geometries are still sparse. Among the studies in ideal stenotic districts, we cite e.g. Razavi et al [24], who studied different non-Newtonian models in a 2D idealized stenotic carotid, and Chen et al [6], who studied an ideal model of stenotic coronary artery treated with an end-to-side bypass graft. As for coronary bypasses, we mention Kabinejadian et al [15], who studied a compliant model of an idealized sequential coronary artery bypass graft, but without including the stenosis in the 3D geometry. Even more rare are the studies on patient-specific stenotic vessels: Stroud et al [30] compared Newtonian and non-Newtonian models in a severely stenotic patient-specific carotid, but only a two-dimensional model was examined; Shirmer et al [27] studied a 3D patient-specific stenotic carotid artery, but no comparison was made with the Newtonian model; Vimmr et al

[33] performed a numerical comparison of Newtonian and non-Newtonian models in patient-specific aorto-coronary bypasses. At the best of our knowledge, no comparisons between Newtonian and non-Newtonian models have been made so far in patient-specific 3D stenotic carotid arteries. Furthermore, no attention has been given to the influence of the degree of stenosis on the non-Newtonian behavior of blood in 3D patient-specific aorto-coronary bypass configurations.

In this context, the aim of this work is to investigate the effects of non-Newtonian blood rheology on the hemodynamics of 3D patient-specific stenotic vessels. In particular, we studied two sets of geometries:

1. two carotid arteries with severe stenosis (i.e. greater than 70%);
2. a stenotic coronary artery treated with a bypass graft. In this case, we virtually vary the degree of stenosis in order to obtain three different degrees of coronary stenosis (50%, 70%, 90%), with the aim of analysing the effects of the non-Newtonian rheology for different degrees of stenosis.

On these geometries, reconstructed from MRI or CT images, we performed unsteady numerical simulations based on the Finite Element method. In order to describe the non-Newtonian blood rheology, we choose the Carreau-Yasuda model, since this model is able to correctly describe the physiological shear-thinning behavior of blood [26].

2 Materials and Methods

2.1 Computational domains and mesh generation

For this study, we consider two carotids with a degree of stenosis greater than 70% who underwent elective carotid endarterectomy, i.e. the surgical removal of atherosclerotic plaque (cases CA1, CA2), and one patient with isolated severe left anterior descending (LAD) coronary artery disease (i.e. stenosis greater than 70%) who underwent aorto-coronary bypass graft surgery by means of the left internal mammary artery (case CO1). Radiological images were acquired by means of Magnetic Resonance technology for CA1 and CA2 and Contrast Enhanced Computed Tomography for CO1.

Using the software VMTK (www.vmtk.org), we reconstructed from the radiological images a surface model of the interface between the blood and the arterial wall (see Figure 1 for two examples of reconstructed surfaces). The corresponding computational domains were turned into volumetric meshes of tetrahedra, obtained after a refinement study (constant wall shear stresses up to a tolerance of 2%). A local mesh refinement was also performed in all the cases at the level of the stenosis. As examples, we report in Figure 2 a detail of the meshes for CA1 and CO1 cases.

2.2 Mathematical and numerical methods

We consider blood as a homogeneous and incompressible fluid described by the Navier-Stokes equations [9] and we assume either a Newtonian or a non-Newtonian rheology model. In particular, for the latter case we choose the *Carreau-Yasuda* model, with viscosity given by [7, 33]

$$\mu(\mathbf{x},t) = \mu_\infty + (\mu_0 - \mu_\infty)\left(1 + (\lambda\dot{\gamma}(\mathbf{x},t)^a\right)^{\frac{n-1}{a}}, \tag{1}$$

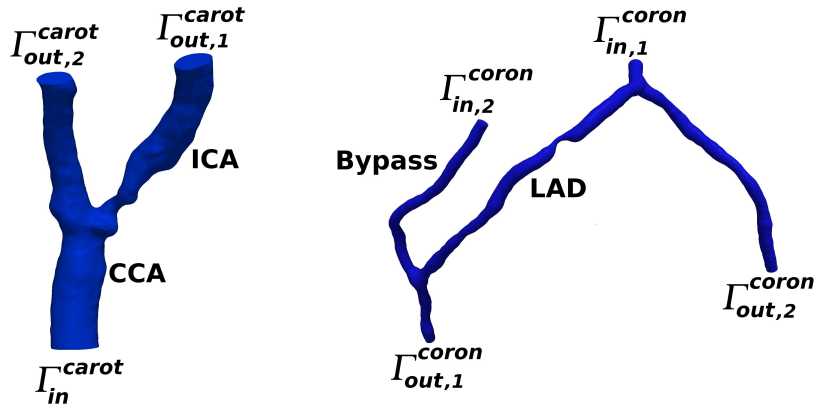

Figure 1: Computational domains for the numerical simulations. Left: case CA2. Right: case CO1 with a 70% LAD stenosis

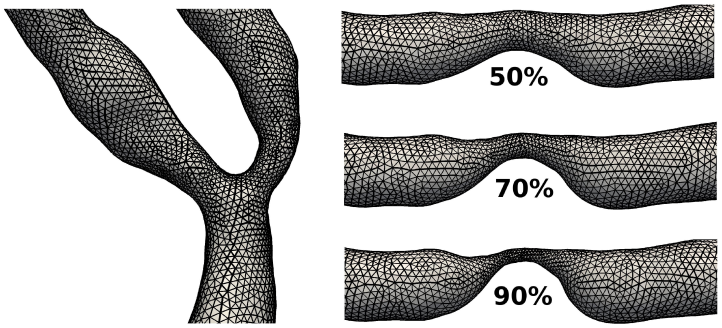

Figure 2: Mesh details. Left: stenotic carotid bifurcation of case CA1. Right: different degrees of LAD stenosis of case CO1

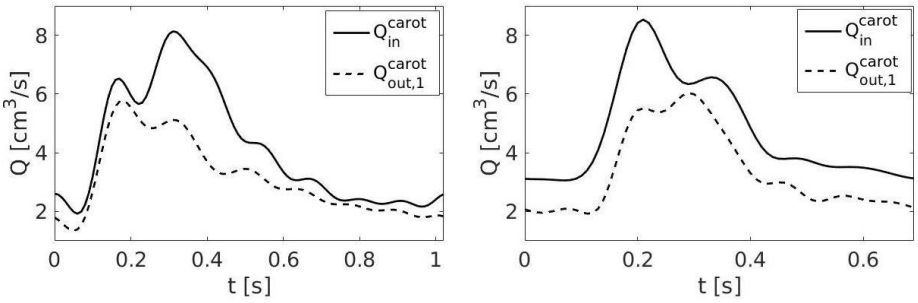

Figure 3: Flow rates imposed as boundary conditions on the inlet and outlet of the computational domain for cases CA1 (left) and CA2 (right)

where $\dot{\gamma}$ is the shear rate defined by $\dot{\gamma} = 2\sqrt{D_{II}}$, $D_{II} = \frac{1}{2}\sum_{i,j=1}^{3} D_{ij}D_{ij}$ being the second invariant of the rate of deformation tensor $\mathbf{D}(\mathbf{u}) = \frac{1}{2}\left(\nabla\mathbf{u} + (\nabla\mathbf{u})^T\right)$, with $\mathbf{u} = \mathbf{u}(\mathbf{x}, t)$ the fluid velocity. For the Newtonian case, we set $\mu = \mu_\infty$. Since the viscosity given by (1) is a function of the velocity, we will write in general $\mu = \mu(\mathbf{u})$. The values of the parameters that define the Carreau-Yasuda model are $\lambda = 1.902s$, $n = 0.22$, $a = 1.25$, $\mu_0 = 0.56\,P$, $\mu_\infty = 0.035\,P$.

As for time discretization, we consider the backward Euler method with a semi-implicit treatment of the convective term. The non-linearity arising from the non-Newtonian model (1) is treated semi-implicitly. This means that, indicating with z^n the approximation of a generic function $z(t)$ evaluated at $t^n = n\Delta t$, $n = 1, \ldots$, at each time-step t^n we have the following discretized-in-time problem to be solved in the computational domain Ω:

$$\begin{cases} \rho\dfrac{\mathbf{u}^n - \mathbf{u}^{n-1}}{\Delta t} - \mu(\mathbf{u}^{n-1})\nabla\cdot\left(\nabla\mathbf{u}^n + (\nabla\mathbf{u}^n)^T\right) + \rho\mathbf{u}^{n-1}\cdot\nabla\mathbf{u}^n + \nabla p^n = \mathbf{0} & \text{in } \Omega, \\ \nabla\cdot\mathbf{u}^n = 0 & \text{in } \Omega, \end{cases}$$

equipped with a suitable initial condition for the velocity, and where $\rho = 1.06 g/cm^3$ is the fluid density and $p = p(\mathbf{x}, t)$ the fluid pressure.

As for the boundary conditions, we consider at each discrete time t^n a flow rate condition

$$\int_\Gamma \mathbf{u}^n \cdot \mathbf{n}\, d\gamma = Q(t^n),$$

for $\Gamma = \Gamma_{in}^{carot}$, $\Gamma_{out,1}^{carot}$, $\Gamma_{in,1}^{coron}$, $\Gamma_{in,2}^{coron}$, $\Gamma_{out,1}^{coron}$ (see Figure 1) and where Q are the corresponding flow rates depicted in Figure 3 for cases CA1 and CA2 and Figure 4 for case CO1 (for each degree of stenosis). For the carotid cases, the patient-specific measures of flow rate were obtained by means of Doppler echocardiography technique (see [11] for more details). For the coronary cases, the prescribed flow rate at the coronary inlet $\Gamma_{in,1}^{coron}$ and at the graft inlet $\Gamma_{in,2}^{coron}$ were taken from literature [16, 25]. For the latter section, the amplitude of the signal was set in accordance to the degree of stenosis, in order to guarantee that the flow rate perfusing the myocardium at the outlet $\Gamma_{out,1}^{coron}$ (calibrated by means of an *healthy* simulation) remained constant, as observed in the clinical practice [21, 22] (see [12] for more details). In the remaining artificial sections

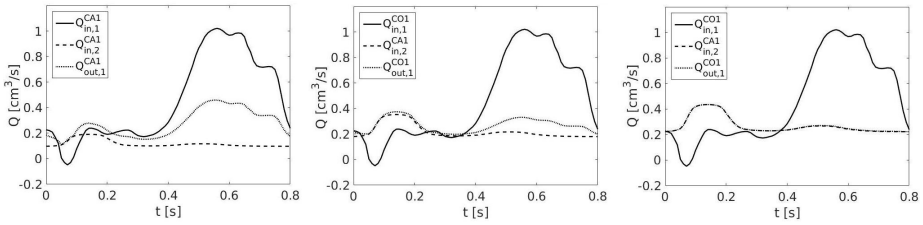

Figure 4: Flow rates imposed as boundary conditions on the inlets and outlet of the computational domain for case CO1 for different degrees of stenosis: 50% (left), 70% (middle) and 90% (right)

$\Gamma_{out,2}^{carot}$ and $\Gamma_{out,2}^{coron}$, the following homogeneous Neumann condition is prescribed, in accordance with the fluid incompressibility:

$$-p^n \mathbf{n} + \mu \left(\mathbf{u}^{n-1}\right) \mathbf{D}\left(\mathbf{u}^n\right) = \mathbf{0}.$$

We performed unsteady numerical simulations using the Finite Element library LifeV developed at MOX - Politecnico di Milano, INRIA - Paris, CMCS - EPF of Lausanne, and Emory University - Atlanta (www.lifev.org). The vessel walls were assumed to be rigid. In order to highlight the differences between Newtonian and non-Newtonian rheologies, we did not consider any turbulence model, although for stenotic carotids transition to turbulence may occur [18, 19]. We used $P1_{bubble} - P1$ finite elements for the space discretization and we set the time discretization parameter $\Delta t = 0.01s$. The flow rate conditions were prescribed by means of a Lagrange multipliers method, see [8, 32].

3 Results

3.1 Carotid arteries

In order to investigate the differences between the Newtonian (N) and non-Newtonian (N-N) models, we report in Figure 5 the velocity magnitude $v(\mathbf{x}, t) = \sqrt{u_x^2 + u_y^2 + u_z^2}$ at the systolic instant t_1 and at the post-systolic instant $t_2 = 0.41\,s$ on selected sections in cases CA1 and CA2, respectively. Furthermore, Figure 6 shows the vorticity magnitude $w(\mathbf{x}, t) = \sqrt{\omega_x^2 + \omega_y^2 + \omega_z^2}$ [1] on the same sections for CA1 and CA2. These sections were selected so as to comprise the common carotid artery (CCA), the stenosis and the internal carotid artery (ICA). In the same images we also report, for t_1 and t_2 and on the same sections, the viscosity computed for the non-Newtonian model and the differences $d_V(\mathbf{x}, t) = |v_N - v_{NN}|$ and $d_w(\mathbf{x}, t) = |w_N - w_{NN}|$, where the subscripts N and NN refer to the Newtonian and non-Newtonian computations, respectively. From these results, small differences can be observed between the two models both for velocity and vorticity at systole (t_1). Instead, some differences are noticeable at t_2: for the velocity, at the distal ICA and, only for case CA2, at the CCA, whereas for the vorticity, mainly at the ICA for both the cases. As

[1] We recall that the vorticity, ω, is defined as $\omega = \nabla \times \mathbf{u}$

Table 2: Mean relative difference computed with (2) between the Newtonian (N) and non-Newtonian (N-N) cases for velocity, vorticity and WSS magnitudes for CA1 and CA2 at t_1 and t_2

	velocity magnitude		vorticity magnitude		WSS magnitude	
	t_1	t_2	t_1	t_2	t_1	t_2
CA1	4.8%	9.1%	5.8%	11.8%	3.6%	6.5%
CA2	9.5%	24.0%	10.9%	30.4%	7.2%	18.4%

for the viscosity in the non-Newtonian cases, we notice higher values in regions where the vessel diameter is large (e.g. in the CCA and in the region downstream the stenosis). This is due to lower velocities and shear rates at larger diameters, which result in higher viscosities due to the *shear-thinning* behavior of blood.

Figure 7 shows the Wall Shear Stress (WSS) magnitude $t_w(\mathbf{x},t) = \sqrt{\tau_{w,x}^2 + \tau_{w,y}^2 + \tau_{w,z}^2}$ at systole for CA1 and CA2, together with the viscosity computed for the non-Newtonian model. The Wall Shear Stress vector, τ_w, is defined as $\tau_w = \mathbf{t} - (\mathbf{t}\cdot\mathbf{n})\mathbf{n}$, where $\mathbf{t} = 2\mu\mathbf{D}\mathbf{n}$ is the traction vector acting on a surface with normal $\mathbf{n}$. Systolic WSS is an important index of risk of plaque rupture (see [28]), so that it is interesting to evaluate the possible effects of the non-Newtonian model on the quantification of this index. From the figures, no significant differences are observed between the Newtonian and non-Newtonian solutions. We notice that the regions where the viscosities are higher correspond to region of low WSS, which however are not regions of interest for stenotic carotids.

We finally report in Table 2 the mean relative differences between the Newtonian (N) and non-Newtonian (N-N) results at instants t_1 and $_2$ for velocity, vorticity and WSS magnitudes, defined as

$$\frac{\int_\Omega |q_N - q_{NN}| d\mathbf{x}}{\int_\Omega |q_N| d\mathbf{x}} \quad q = v, w, t_w. \tag{2}$$

Differences up to nearly 24% and 30% are visible for velocity and vorticity magnitudes, respectively, thus confirming what we observed in Figures 5 and 6. For WSS magnitude, the differences are not so negligible as we inferred from Figure 7. In any case, the differences are more pronounced at the deceleration phase (instant t_2).

3.2 Coronary arteries

Figure 8 shows the diastolic (i.e. the maximum, see Fig. 4) velocity magnitude for the three degrees of stenosis on a selected section at the region of the anastomosis. Furthermore, for the same section, we report the viscosity computed for the non-Newtonian model and the difference d_v between Newtonian and non-Newtonian results. We notice appreciable differences in the viscosity and, accordingly, in the velocity field. In particular, the latter are more localized in the native/stenotic artery (on the right in the figures) for smaller degrees of stenosis and at the anastomosis region for higher degrees of stenosis, and they are more pronounced for higher degree of stenosis. In Table 3, we report the

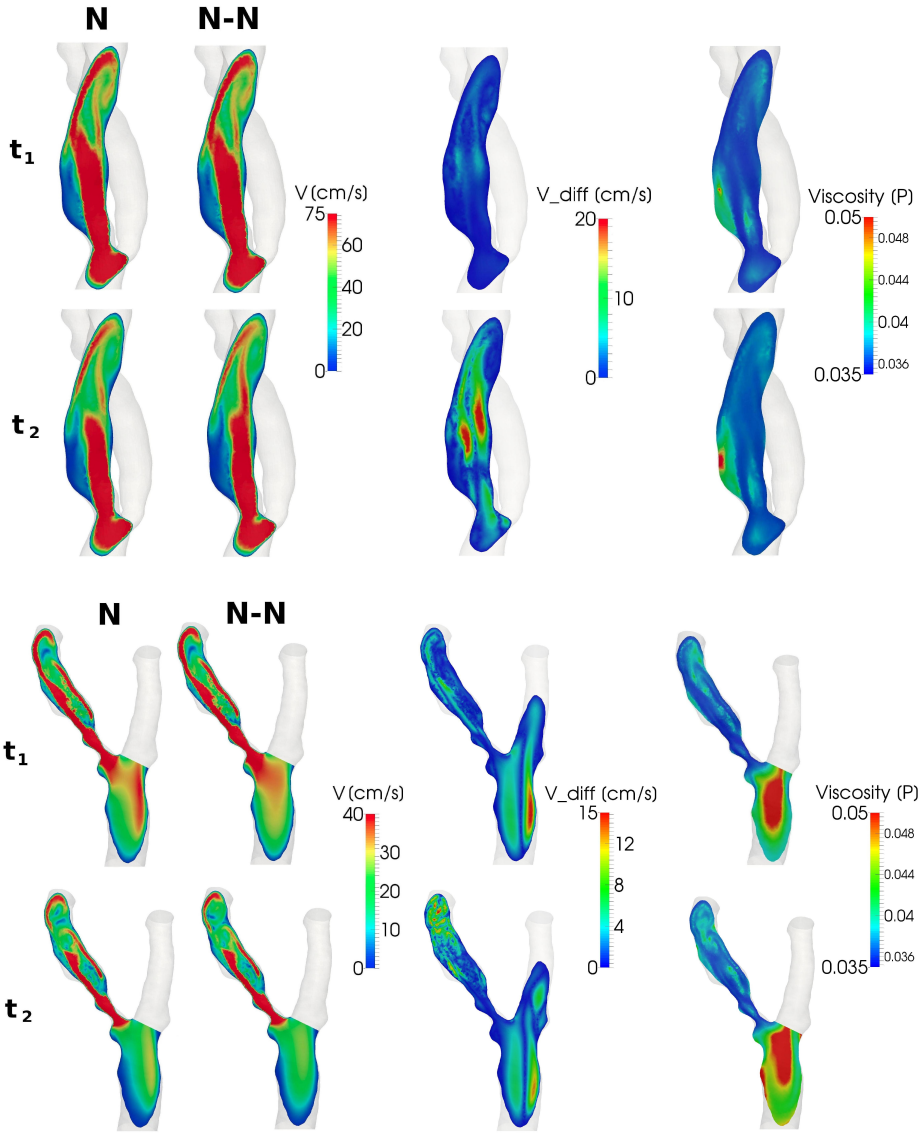

Figure 5: Left columns: Velocity magnitude v in the Newtonian (N) and non-Newtonian (N-N) models. Middle column: Absolute value of the difference between the Newtonian and non-Newtonian velocity magnitudes. Right column: Viscosity computed for the non-Newtonian model. Top: CA1 case; bottom: CA2 case. For each case, the quantities are reported on a selected section and at the systolic (t_1) and post-systolic (t_2) instants

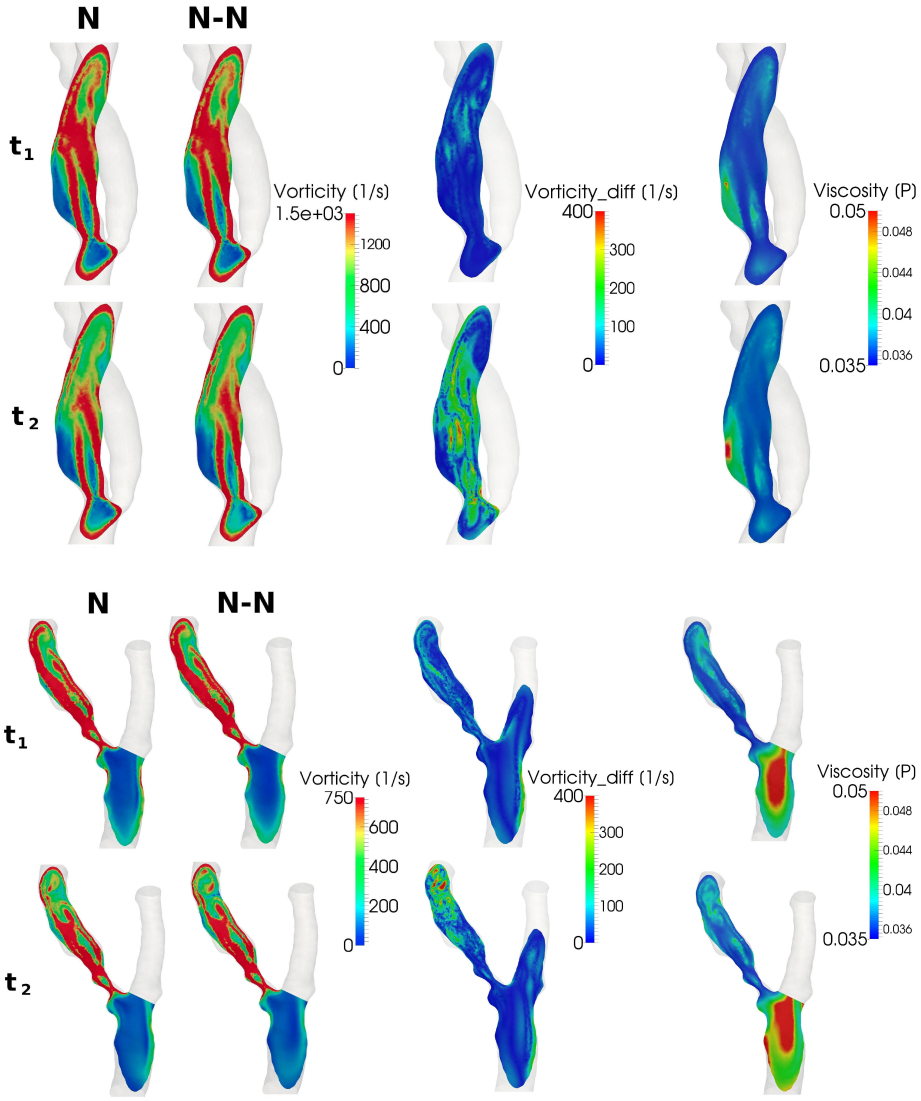

Figure 6: Left columns: Vorticity magnitude w in the Newtonian (N) and non-Newtonian (N-N) models. Middle column: Absolute value of the difference between the Newtonian and non-Newtonian vorticity magnitudes. Right column: Viscosity computed for the non-Newtonian model. Top: CA1 case; bottom: CA2 case. For each case, the quantities are reported on a selected section and at the systolic (t_1) and post-systolic (t_2) instants

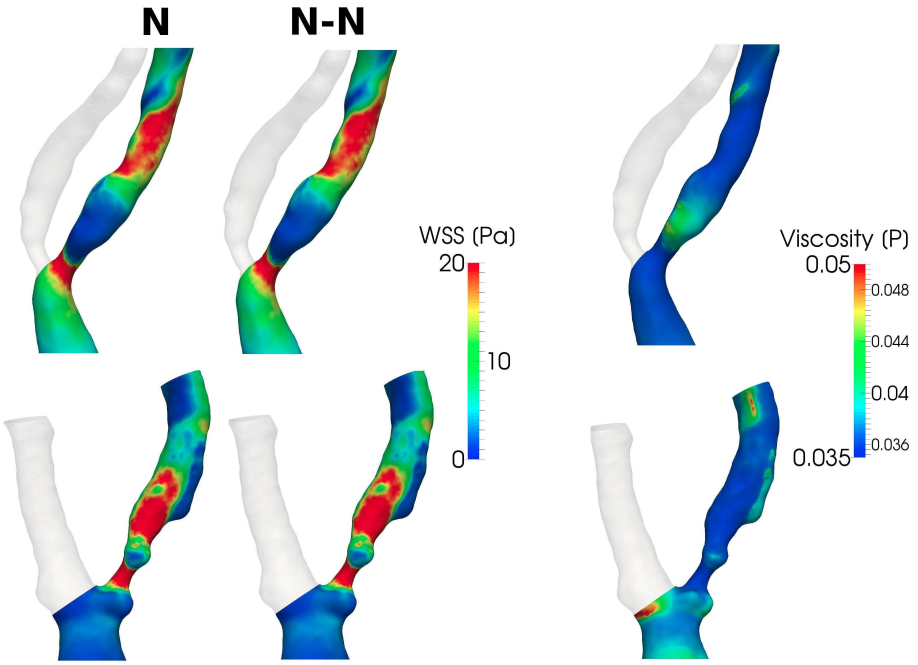

Figure 7: WSS magnitude at the systolic instant t_1 in the Newtonian (N) and non-Newtonian (N-N) models. Top: case CA1; bottom: case CA2. The viscosity computed for the non-Newtonian model is also reported

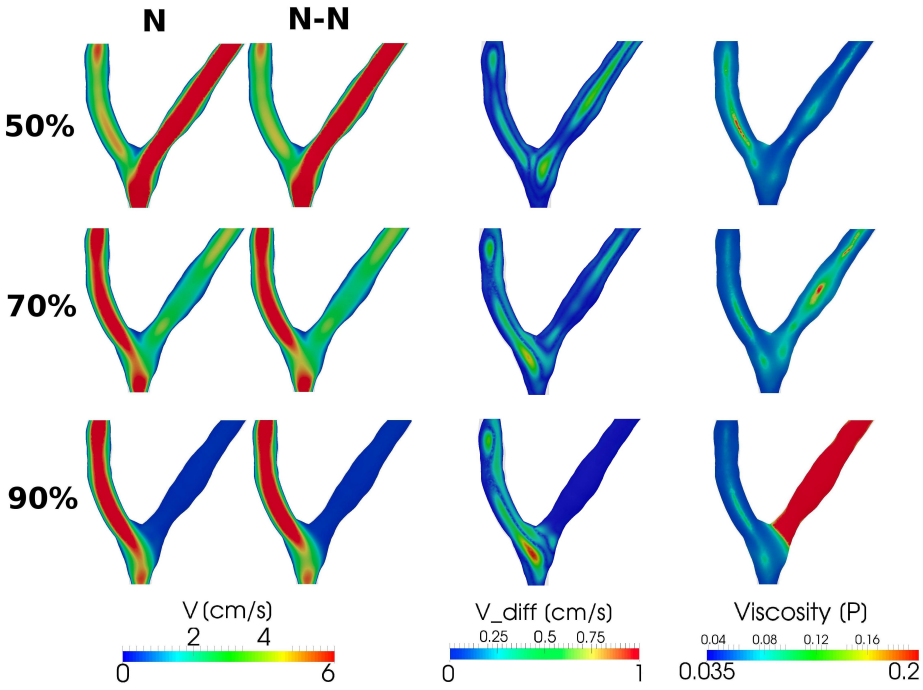

Figure 8: Left columns: velocity magnitude v in the Newtonian (N) and non-Newtonian (N-N) models. Middle column: absolute value of the difference between the Newtonian and non-Newtonian velocity magnitudes. Right column: viscosity computed for the non-Newtonian model. Top: 50% degree of stenosis; middle: 70% degree of stenosis; bottom: 90% degree of stenosis. For each case, the quantities are reported on a selected section and at the diastolic instant

Table 3: Mean relative difference computed with (2) between the Newtonian (N) and non-Newtonian (N-N) cases for the diastolic velocity magnitude and RRT for different degrees of stenosis

% stenosis	velocity magnitude	RRT
50%	2.7%	34.3%
70%	2.8%	51.5%
90%	6.9%	91.5%

mean relative differences of diastolic velocity magnitude given by (2), $q = v$. These results confirm that the relative difference increases for increasing values of the stenosis degree.

In Figure 9, we report the Relative Residence Time (RRT) distribution in a region comprising the coronary-bypass anastomosis and the stenosis for Newtonian and non-Newtonian models and for each degree of stenosis. RRT is a function of space defined on the lumen boundary given by

$$RRT(\mathbf{x}) = \frac{1}{(1 - 2OSI(\mathbf{x}))TAWSS(\mathbf{x})},$$

where OSI is the Oscillatory Shear Index

$$OSI(\mathbf{x}) = \frac{1}{2}\left(1 - \frac{\left\|\int_0^T \tau_w(t,\mathbf{x})dt\right\|}{\int_0^T \|\tau_w(t,\mathbf{x})\|\,dt}\right),$$

and $TAWSS$ is the Time-Averaged Wall Shear Stress

$$TAWSS(\mathbf{x}) = \frac{1}{T}\int_0^T \|\tau_w(t,\mathbf{x})\|\,dt.$$

The choice of this index for the comparison between the models was driven by the fact that RRT is known to be related to the risk of plaque formation in coronary arteries [17] and, since restenosis is a known clinical problem in coronary artery bypasses (see [2]), it is interesting to investigate the effects of the non-Newtonian model on this index. We can see from the figure that RRT is greatly influenced by the choice of the rheological model for all stenosis degrees (notice that the scales are different for each stenosis degree, in order to better emphasize the differences). In particular, the Newtonian model overestimates RRT, especially at the anastomosis and in the native/stenotic branch. The reason for these differences may be attributed to the low flow rates in the stenotic vessel (in addition to the generally low flow rates in the coronary arteries), thus featuring very low shear rates. These results are also confirmed by the mean relative differences of RRT computed owing to (2), $q = RRT$, which are reported in Table 3 for each degree of stenosis and which feature very high values, especially for increasing values of the stenosis degree.

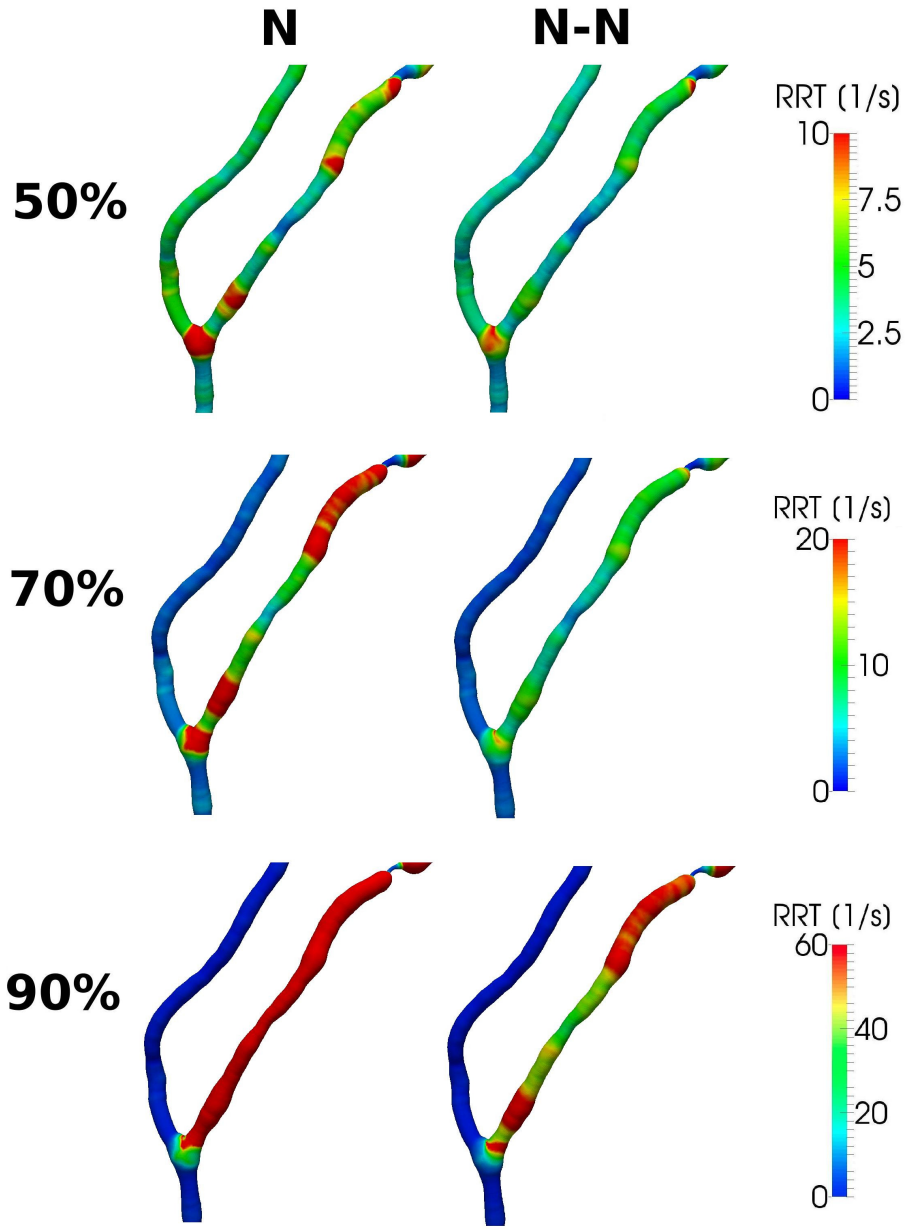

Figure 9: RRT distribution in a region comprising the coronary-bypass anastomosis and the stenosis in the Newtonian (N) and non-Newtonian (N-N) cases for each degree of stenosis, case CO1

4 Conclusions

The purpose of this study was to investigate the influence of non-Newtonian blood rheology in stenotic vessels. In particular, we considered two carotid arteries with severe stenosis (i.e. greater than 70%) and one coronary vessel in which we virtually varied the stenosis degree (50%, 70%, 90%). Our comparisons between Newtonian and non-Newtonian models showed that:

1. for stenotic carotid arteries, velocity and vorticity fields are influenced by blood rheology (mean differences of magnitudes up to 24% and 30%, respectively). Smaller differences were found in the quantification of WSS (mean difference of magnitude up to 18%);

2. also for stenotic coronary arteries, the velocity field is influenced by blood rheology. Moreover, great differences were found in the quantification of RRT (for all stenosis degrees). Thus, we believe that the non-Newtonian behavior of blood should not be neglected to accurately compute RRT, regardless of the degree of the stenosis.

Limitations of this work are the absence of turbulence models in the stenotic carotids and of a fluid-structure interaction model. We are working on both these topics to understand their importance in quantifying the differences between Newtonian and non-Newtonian models.

References

[1] O. K. Baskurt and H. J. Meiselman. Blood rheology and hemodynamics. *Semin. Thromb. Hemost.*, 29(5):435–450, 2003.

[2] A. Berger, P. A. MacCarthy, U. Siebert, S. Carlier, W. Wijns, G. Heyndrickx, J. Bartunek, H. Vanermen, and B. D. Bruyne. Long-term patency of internal mammary artery bypass grafts - Relationship with preoperative severity of the native coronary artery stenosis. *Circulation*, 110:36–40, 2004.

[3] N. Bessonov, A. Sequeira, S. Simakov, Y. Vassilevskii, and V. Volpert. Methods of blood flow modelling. *Math. Model. Nat. Phenom.*, 11(1):1–25, 2006.

[4] F. M. Box, R. J. van der Geest, M. C. Rutten, and R. J. H. The influence of flow, vessel diameter, and non-Newtonian blood viscosity on the wall shear stress in a carotid bifurcation model for unsteady flow. *Invest. Radiol.*, 40(5):277–94, 2005.

[5] J. Boyd and J. Buick. Comparison of Newtonian and non-Newtonian flows in a two dimensional carotid artery model using the lattice Boltzmann method. *Phys. Med. Biol.*, 52(20):6215–6228, 2007.

[6] J. Chen, X.-Y. Lu, and W. Wang. Non-newtonian effects of blood flow on hemodynamics in distal vascular graft anastomoses. *J. Biomech.*, 39:1983–1995, 2006.

[7] Y. I. Cho and K. R. Kensey. Effects of the non-Newtonian viscosity of blood on flows in a diseased arterial vessel. *Biorheology*, 28:241–262, 1991.

[8] L. Formaggia, J. F. Gerbeau, F. Nobile, and A. Quarteroni. Numerical treatment of defective boundary conditions for the Navier-Stokes equation. *SIAM J. Numer. Anal.*, 40(1):376–401, 2002.

[9] L. Formaggia, A. Quarteroni, and A. Veneziani. *Cardiovascular Mathematics: Modeling and Simulation of the Circulatory System, Modeling, Simulation and Application*. Springer, 2009.

[10] F. J. H. Gijsen, F. N. van de Vosse, and J. D. Janssen. The influence of the non-newtonian properties of blood on the flow in large arteries: steady flow in a carotid bifurcation model. *J. Biomech.*, 32(6):601–608, 1999.

[11] B. Guerciotti, C. Vergara, L. Azzimonti, L. Forzenigo, A. Buora, P. Biondetti, and M. Domanin. Computational study of the fluid-dynamics in carotis before and after endarterectomy. *J. Biomech.*, 49:26–38, 2016.

[12] B. Guerciotti, C. Vergara, S. Ippolito, A. Quarteroni, C. Antona, and R. Scrofani. Computational study of the risk of restenosis in coronary bypasses. MOX-Report n. 13-2016, MOX, Politecnico di Milano, 2016.

[13] W. W. Jeong and K. Rhee. Effects of surface geometry and non-newtonian viscosity on the flow field in arterial stenoses. *J. Mech. Sci. Technol.*, 23:2424–2433, 2009.

[14] B. M. Johnston, P. R. Johnston, S. Corney, and D. Kilpatrick. Non-Newtonian blood flow in human right coronary arteries: transient simulations. *J. Biomech.*, 39:1116–1128, 2006.

[15] F. Kabinejadian and D. N. Ghista. Compliant model of a coupled sequential coronary arterial bypass graft: effects of vessel wall elasticity and non-newtonian rheology on blood flow regime and hemodynamic parameters distribution. *Med. Eng. Phys.*, 34:860–872, 2012.

[16] J. Keegan, P. D. Gatehouse, G. Z. Yang, and D. N. Firmin. Spiral phase velocity mapping of left and right coronary artery blood flow: correction for through-plane motion using selective fat-only excitation. *J. Magn. Reson. Im.*, 20:953–960, 2004.

[17] J. Knight, U. Olgac, S. C. Saur, D. Poulikakos, W. J. Marshall, P. C. Cattin, H. Alkadhi, and V. Kurtcuoglu. Choosing the optimal wall shear parameter for the prediction of plaque location - A patient-specific computational study in human right coronary arteries. *Atherosclerosis*, 211(2):445–450, 2010.

[18] R. M. Lancellotti, C. Vergara, L. Valdettaro, S. Bose, and A. Quarteroni. Large eddy simulations for blood fluid-dynamics in real stenotic carotids. MOX-Report n. 63-2015, MOX, Politecnico di Milano, 2015.

[19] S. Lee, S. Lee, P. Fischer, H. Bassiouny, and F. Loth. Direct numerical simulation of transitional flow in a stenosed carotid bifurcation. *J Biomech*, 41(11):2551–2561, 2008.

[20] B. Liu and D. Tang. Influence of non-Newtonian properties of blood on the wall shear stress in human atherosclerotic right coronary arteries. *Mol. Cell. Biomech.*, 8(1):73–90, 2011.

[21] X. Meng, Q. Fu, W. Sun, J. Yu, Y. W, and W. Bi. Competitive flow arising from varying degrees of coronary artery stenossi affects the blood flow and the production of nitric oxide and endothelin in the internal mammary artery. *Eur. J. Cardio-Thorac.*, 43:1022–1027, 2013.

[22] S. Pagni, J. Storey, J. Ballen, W. Montgomery, B. Y. Chiang, S. Etoch, and P. A. Spence. ITA versus SVG: a comparison of instantaneous pressure and flow dynamics during competitive flow. *Eur. J. Cardio-Thorac.*, 11:1086–1092, 1997.

[23] K. Perktold, R. O. Peter, M. Resch, and G. Langs. Pulsatile non-Newtonian blood flow in a three-dimensional carotid bifurcation models: a numerical sudy of flow phenomena under different bifurcation angles. *J. Biomed. Eng.*, 13(6):507–515, 1991.

[24] A. Razavi, E. Shirani, and M. R. Sadeghi. Numerical simulation of blood pulsatile flow in a stenosed carotid artery using different rheological models. *J. Biomech.*, 44(11):2021–2030, 2011.

[25] H. Sakuma, S. Globits, M. O'Sullivan, A. Shimakawa, M. A. Berstein, T. K. F. Foo, T. M. Amidon, K. Takeda, T. Nakagawa, and C. B. Higgins. Breath-hold MR measurements of blood flow velocity in internal mammary arteries and coronary artery bypass grafts. *J. Magn. Reson. Im.*, 1:219–222, 1996.

[26] S. S. Shibeshi and W. E. Collins. The rheology of blood flow in a branched arterial system. *Appl Rheo*, 15(6):398–405, 2005.

[27] C. M. Shirmer and A. M. Malek. Computational fluid dynamic characterization of carotid bifurcation stenosis in patient-based geometries. *Brain Behav.*, 2(1):45–52, 2012.

[28] C. Slager, J. Wentzel, F. Gijsen, J. Schuurbiers, A. van der Wal, A. van der Steen, and P. Serruys. The role of shear stress in the generation of rupture-prone vulnerable plaques. *Nature Reviews Cardiology*, 2(9):401–407, 2005.

[29] J. V. Soulis, G. D. Giannoglou, Y. S. Chatzizsis, K. V. Seralidou, G. E. Parcharidis, and G. E. Louridas. Non-Newtonian models for molecular viscosity and wall shear stress in a 3D reconstructed human left coronary artery. *Med. Eng. Phys.*, 30:9–19, 2008.

[30] J. S. Stroud, S. A. Berger, and D. Saloner. Numerical analysis of flow through a severely stenotic carotid artery bifurcation. *J. Biomech. Eng.*, 124(1):9–20, 2002.

[31] A. Valencia, A. Zarate, M. Galvez, and L. Badilla. Non-newtonian blood flow dynamics in a right internal carotid artery with a saccular aneurysm. *Int. J. Numer. Meth. Fl.*, 50:751–764, 2006.

[32] A. Veneziani and C. Vergara. Flow rate defective boundary conditions in haemodynamics simulations. *Int. J. Numer. Meth. Fl.*, 47:803–816, 2005.

[33] J. Vimmr, A. Jonašóvá, and O. Bublík. Numerical analysis of non-Newtonian blood flow and wall shear stress in realistic single, double and triple aorto-coronary bypasses. *Int. J. Numer. Method Biomed. Eng.*, 29:1057–1081, 2013.

MOX Technical Reports, last issues

Dipartimento di Matematica
Politecnico di Milano, Via Bonardi 9 - 20133 Milano (Italy)

18/2016 Ferroni, A.; Antonietti, P.F.; Mazzieri, I.; Quarteroni, A.
Dispersion-dissipation analysis of 3D continuous and discontinuous spectral element methods for the elastodynamics equation

17/2016 Penati, M.; Miglio, E.
A new mixed method for the Stokes equations based on stress-velocity-vorticity formulation

15/2016 Ieva, F.; Paganoni, A.M.
A taxonomy of outlier detection methods for robust classification in multivariate functional data

16/2016 Agosti, A.; Antonietti, P.F.; Ciarletta, P.; Grasselli, M.; Verani, M.
A Cahn-Hilliard type equation with degenerate mobility and single-well potential. Part I: convergence analysis of a continuous Galerkin finite element discretization.

14/2016 Bonomi, D.; Manzoni, A.; Quarteroni, A.
A matrix discrete empirical interpolation method for the efficient model reduction of parametrized nonlinear PDEs: application to nonlinear elasticity problems

13/2016 Guerciotti, B; Vergara, C; Ippolito, S; Quarteroni, A; Antona, C; Scrofani, R.
Computational study of the risk of restenosis in coronary bypasses

12/2016 Bartezzaghi, A.; Dedè, L.; Quarteroni, A.
Isogeometric Analysis of Geometric Partial Differential Equations

11/2016 Zhu, S.; Dedè, L.; Quarteroni, A.
Isogeometric Analysis and proper orthogonal decomposition for the acoustic wave equation

10/2016 Flemisch, B.; Fumagalli, A.; Scotti, A.
A review of the XFEM-based approximation of flow in fractured porous media

08/2016 Dassi, F.; Perotto, S.; Si, H.; Streckenbach, T.
A priori anisotropic mesh adaptation driven by a higher dimensional embedding